Langmuir
Letter
pubs.acs.org/Langmuir

Peptide Nanotube Nematic Phase

S. Bucak,*[,†] C. Cenker,[‡] I. Nasir,[†,‡] U. Olsson,[‡] and M. Zackrisson[‡,§]

[†]*Department of Chemical Engineering, Yeditepe University, Istanbul, Turkey and* [‡]*Physical Chemistry 1, Lund University, Box 124, SE-221 00 Lund, Sweden.* [§] *Present address: The Adolphe Merkle Institute, Université de Fribourg Rte de l'Ancienne Papeterie, Box 209, CH-1723 Marly, Switzerland*

Received December 18, 2008. Revised Manuscript Received February 7, 2009

The self-assembly of the trifluoroacetate salt of the short peptide $(ala)_6$-lys (A_6K) in water has been investigated by cryo-transmission electron microscopy and small-angle X-ray scattering. For concentrations below ca. 12%, the peptide does not self-assemble but forms a molecularly dispersed solution. Above this critical concentration, however, A_6K self-assembles into several-micrometer-long hollow nanotubes with a monodisperse cross-sectional radius of 26 nm. Because the peptides carry a positive charge, the nanotubes are charge-stabilized. Because of the very large aspect ratio, the tubes form an ordered phase that presumably is nematic.

Introduction

The development of modern peptide chemistry[1,2] has opened the possibility of custom peptide synthesis that allows for systematically investigating the relationship between a specific oligopeptide molecular structure and the macroscopic phases and structures formed in such systems.[3−5] Understanding the assembly behavior of peptides is important not only in designing nanomaterials for a desired functionality[6,7] but also in combating neurodegenerative diseases such as Alzheimer's and Parkinson's, which are strongly associated with an accumulation of amyloid-forming peptides in the brain.[8,9]

Several peptides have been found to undergo self-assembly into various morphologies and structural length scales. Much work has naturally focused on the amyloid-forming peptides, or selected fragments of these, because of the close connection to neurodegenerative diseases. However, several synthetic oligopeptides have also been shown to self-assemble. Generally, β-sheet formation through hydrogen bonding is the basis of peptide self-assembly, resulting in ribbons, tapes, and sometimes nanotubes. These structures may further aggregate or precipitate as fibrils, as in amyloid formation. If properly stabilized, however, stable self-assemblies may be obtained where ribbons or tapes may entangle, forming a viscoelastic solution of "living polymers", and more rigid nanotubes may form ordered nematic or hexagonal phases.

It has also been suggested that certain amphiphilic or surfactant-like peptides may self-assemble because of hydrophobic interactions. Depending on the peptide, one observes micelle formation[10] or peptide bilayers forming spherical or tubular vesicles.[11,12]

It is difficult to determine the local peptide organization in these structures. Valéry et al. were able to obtain detailed structural information on nanotubes of the lanreotide peptide on the basis of high-resolution fiber diffraction data.[13] In analyzing the ordered structure, they found that the tube wall was made up of parallel helical β-sheet ribbons in two layers, giving a bilayer structure. A similar helical ribbon structure has been proposed in another system, although with a slight polydispersity in the number of layers.[14]

In the case of rigid nanotubes, one expects the formation of ordered nematic or hexagonal phases driven by excluded volume interactions. Such ordering is also of interest from an application point of view because it allows for aligning the nanotubes using an external field, such as shear. Ordered phases, however, have until now been identified in only a few systems.[13−15]

In this letter, we report on the self-assembly structures formed by short synthetic oligopeptide A_6K in water, including the formation of liquid-crystalline, presumably nematic, ordering. The self-assembly structures are investigated using cryo-transmission electron microscopy (cryo-TEM) and small-angle X-ray scattering (SAXS). Cryo-TEM has an advantage over ordinary TEM or SEM in that it allows the imaging of the real solution structure at the given composition, not only its solid content after drying. Although there are some reports on peptide nanotubes, to our knowledge this is the first time that cryo electron microscopy data has been available for these kinds of systems, and the data presented in this letter explicitly show the 3D nanotubes of a certain size in great detail.

*To whom correspondence should be addressed. E-mail: seyda@yeditepe.edu.tr.

(1) Merrifield, R. B. *J. Am. Chem. Soc.* **1963**, *85*, 2149–2154.
(2) Howl, J. *Peptide Synthesis and Applications*; Humana Press: Totawa, NJ, **2005**.
(3) Gazit, E. *Chem. Soc. Rev.* **2007**, *36*, 1263–1269.
(4) Ulijn, R. V.; Smith, A. M. *Chem. Soc. Rev.* **2008**, *37*, 664–675.
(5) Zhao, X. A.; Zhang, S. G. *Macromol. Biosci.* **2007**, *7*, 13–22.
(6) Pouget, E.; Dujardin, E.; Cavalier, A.; Moreac, A.; Valery, C.; Marchi-Artzner, V.; Weiss, T.; Renault, A.; Paternostre, M.; Artzner, F. *Nat. Mater.* **2007**, *6*, 434–439.
(7) Reches, M.; Gazit, E. *Science* **2003**, *300*, 625–627.
(8) Harper, J. D. *BMC Chem. Biol.* **1997**, *4*, 119–125.
(9) Walsh, D. M.; Lomakin, A.; Benedek, G. B.; Condron, M. M.; Teplow, D. B. *J. Biol. Chem.* **1997**, *272*, 22364–22372.
(10) Dong, H.; Paramonov, S. E.; Aulisa, L.; Bakota, E. L.; Hartgerink, J. D. *J. Am. Chem. Soc.* **2007**, *129*, 12468–12472.
(11) Soto, P.; Griffin, M. A.; Shea, J. E. *Biophys. J.* **2007**, *93*, 3015–3025.
(12) Zhang, S. G.; Holmes, T.; Lockshin, C.; Rich, A. *Proc. Natl. Acad. Sci. U.S.A.* **1993**, *90*, 3334–3338.
(13) Valery, C.; Paternostre, M.; Robert, B.; Gulik-Krzywicki, T.; Narayanan, T.; Dedieu, J. C.; Keller, G.; Torres, M. L.; Cherif-Cheikh, R.; Calvo, P.; Artzner, F. *Proc. Natl. Acad. Sci. U.S.A.* **2003**, *100*, 10258–10262.
(14) Krysmann, M. J.; Castelletto, V.; McKendrick, J. E.; Clifton, L. A.; Hamley, I. W.; Harris, P. J. F.; King, S. M. *Langmuir* **2008**, *24*, 8158.
(15) Aggeli, A.; Nyrkova, I. A.; Bell, M.; Harding, R.; Carrick, L.; McLeish, T. C. B.; Semenov, A. N.; Boden, N. *Proc. Natl. Acad. Sci. U.S.A.* **2001**, *98*, 11857–11862.

Experimental Section

The trifluoroacetate (tfa) salt of the peptide (alanine)$_6$-lysine (A_6K, 97% purity) was purchased from CPC Scientific, Inc. and used without further purification. This salt will be referred to as (tfa)$_2$-A_6K. Heavy water, D_2O (99.8%), was obtained from Armar Chemicals. Samples were studied in D_2O rather than in H_2O because of NMR measurements that will be reported elsewhere. The peptide concentration here will be given as a volume fraction, ϕ. The peptide density is approximated to be the same as that of D_2O, in which case volume and weight fractions are equal.

Optical microscopy measurements were performed on a Zeiss Axioplan Universal microscope equipped with crossed polarizers.

Cryo-TEM images were taken at the National Center for High Resolution Electron Microscopy at the Chemical Center at Lund University. To improve the wetting properties, the grids were treated by glow discharge, which temporarily forces the hydrophobic surface of the carbon grid to become more hydrophilic. Samples were placed on the grids after glow discharge, followed by fast dipping of the grids in liquid ethane and transfer to liquid nitrogen. Grids were kept in liquid nitrogen prior to imaging.

Small-angle X-ray scattering experiments were conducted on beamline I711 at the MAX II storage ring in Lund, Sweden, using a sample-to-detector distance of 1.5 m and a wavelength of $\lambda = 1.025$ Å. For details regarding the experimental setup, see ref 16. Samples were carefully loaded, using syringes, into high-quality quartz capillaries, supplied by Jan Skov Pedersen, University of Aarhus. Having the capillaries rigidly mounted in cylindrical steel housings allows for long-time use and subtraction of the correct capillary background contribution. Before and after measurements, the sample-containing capillaries were inspected carefully under a microscope to check for any trapped air bubbles. In the data reduction, the decay of the intensity of the primary beam and the transmission of samples were taken into account by measuring the beam intensity with a semiconducting diode immediately before and after sample exposure.

Results and Discussion

A partial phase diagram of the (tfa)$_2$-A_6K water system is presented in Figure 1 for the concentration range $\phi = 0-0.2$, with ϕ being the volume fraction. At low concentrations, the salt, (tfa)$_2$-A_6K, is fully soluble in water on a single-oligomer level, and the solutions are isotropic and transparent. This isotropic liquid phase, L, is stable up to $\phi \approx 0.12$. Above this concentration, a new phase is formed, as manifested in a sharp increase in sample turbidity, and a birefringent texture is observed when viewed between crossed polarizers. In the schematic phase map in Figure 1, a light-microscope image obtained with crossed polarizers is shown. The high-concentration phase, N, is suggested to be a nematic phase, as discussed further below.

In the high-concentration phase, the peptide self-assembles into very long, hollow nanotubes, as seen by the cryo-TEM images presented in Figure 2, obtained at a concentration of $\phi = 0.15$. In Figure 2a, a lower-magnification image is shown, where tubes that are several micrometers long can be observed. Figure 2b shows the tubes at a higher magnification, and here it can clearly be seen that the tubes are hollow with very thin walls. From the image, the tube radius is estimated to be 28 nm. The thin walls may correspond to a single peptide monolayer. However, this is not firmly established because it is not possible to obtain an accurate value for the thickness from these images. The tubes appear to be cylindrical. However, they seem to be slightly deformed by confinement to the grid. In some places, the tubes need to bend over the carbon matrix, which may result in some flattening of the tube and a slight overestimation of the tube radius.

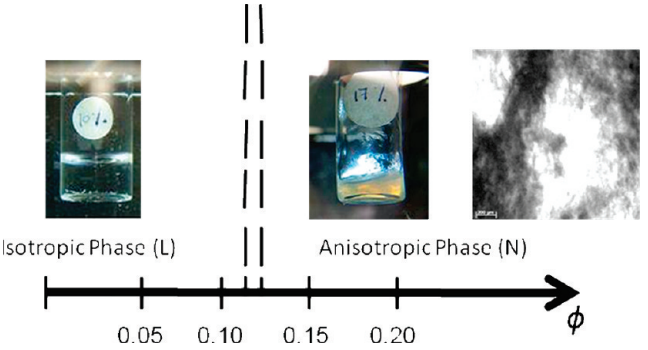

Figure 1. Partial phase map of the water/(tfa)$_2$-A_6K system. At lower concentrations, the isotropic liquid phase (L) is stable. Above ca. $\phi = 0.12$, the system spontaneously forms a nematic phase of long, hollow nanotubes. The texture of the nematic phase as seen in a microscope between crossed polarizers is also shown. The light-microscopy image (1.2 × 1.2 mm^2) refers to a $\phi = 0.25$ sample.

As complementary experiments to investigate the structure, small-angle X-ray scattering (SAXS) experiments were also performed. In these experiments, the sample is injected into a 1 mm cylindrical capillary where no confinement effects on the local structure are expected. In Figure 3, SAXS patterns obtained at peptide concentrations of $\phi = 0.10$ and 0.17 are presented. Here, $I(q)$ is the scattering intensity and q is the magnitude of the scattering vector. It can clearly be seen that the two scattering curves are very different. At the lower concentration, the intensity is very low, and the variation with q is very weak. This implies that the peptides do not self-assemble at this concentration. The best fit using the Guinier expression

$$I(q) \approx \exp\left(-\frac{q^2 {R_g}^2}{3}\right) \quad (1)$$

is shown as a solid line. Here, R_g is the radius of gyration, and from the fit $R_g = 0.44$ nm is obtained, which can be compared with the peptide contour length of approximately 2.5 nm. Whereas the R_g value is associated with a large uncertainty because of the low scattering intensity, it nevertheless demonstrates the absence of any self-assembly at this concentration.

The scattering intensity from the $\phi = 0.17$ sample, which is located in the liquid-crystalline phase, is much higher. At the low-q end, the scattering intensity is approximately 2 orders of magnitude higher. At this concentration, the peptides have self-assembled into nanotubes, and the particular scattering pattern corresponds to the form factor of the nanotubes. At the limit of a very thin wall, the isotropic average form factor, $P(q)$, of long, hollow cylinders is given by

$$P(q) \propto \frac{{J_0}^2(qR)}{q} \quad (2)$$

where J_0 is the zeroth-order Bessel function and R is the tube radius. J_0^2 is the tube form factor perpendicular to the tube's long axis, and the q^{-1} term arises from the isotropic averaging of the tube orientation with respect to a laboratory coordinate

(16) Knaapila, M.; Svensson, C.; Barauskas, J.; Zackrisson, M.; Nielsen, S. S.; Toft, K. N.; Vestergaard, B.; Arleth, L.; Olsson, U.; Pedersen, J. S.; Cerenius, Y., submitted **2008**.

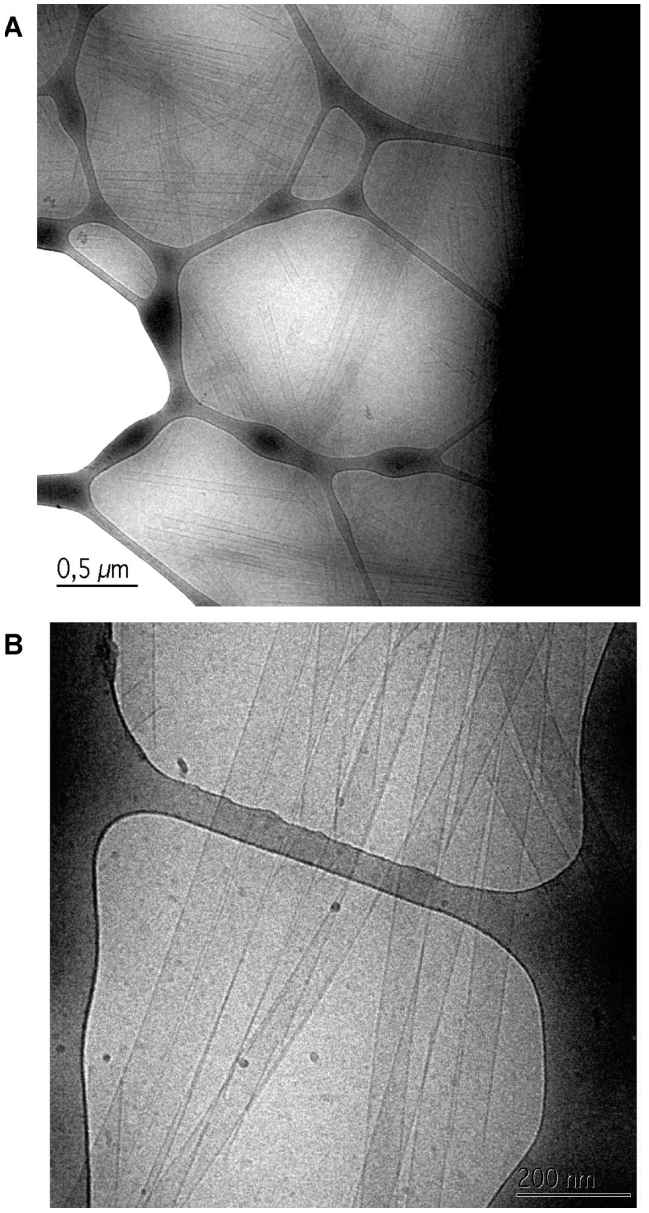

Figure 2. Cryo-TEM images of a $\phi = 0.15$ sample showing very long, hollow nanotubes. (a) Image at lower magnification (bar = 0.5 μm) showing the total length of the nanotubes. (b) Image at higher magnification (bar = 200 nm) showing that the tubes are hollow with thin walls and have a radius of ca. 25−30 nm.

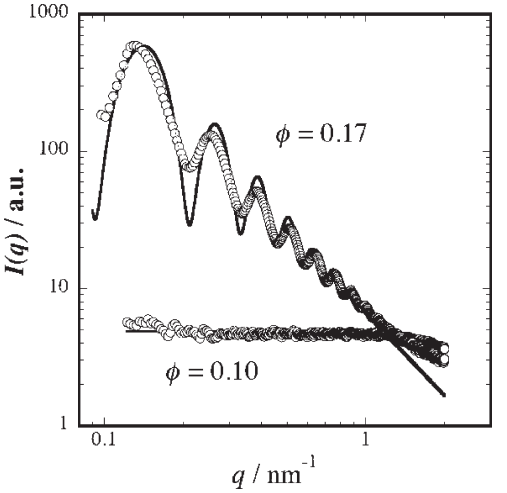

Figure 3. SAXS patterns obtained from the isotropic liquid phase at $\phi = 0.10$ and from the liquid-crystalline phase at $\phi = 0.17$. For $\phi = 0.17$, we note the large number of successive form factor maxima and minima demonstrating a very small variation in tube radius. The solid line here is the calculated scattering from infinitely thin tubes having an average radius of 26 nm with a relative standard deviation of 8% assuming a Gaussian size distribution.

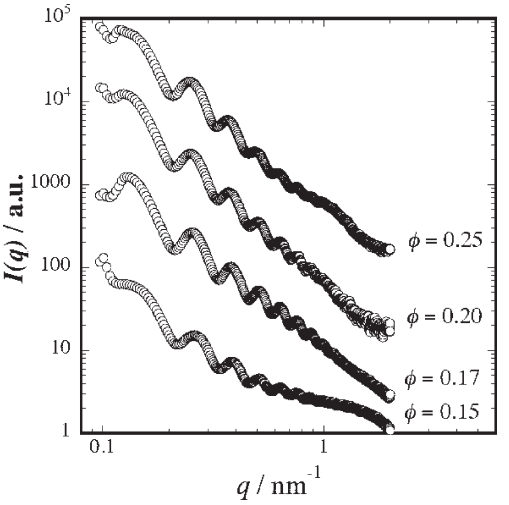

Figure 4. SAXS patterns obtained at different concentrations: $\phi = 0.15$, 0.17, 0.20, and 0.25, respectively. The scattering patterns are very similar, showing that the nanotube radius, 26 nm, is essentially independent of the peptide concentration in this concentration regime.

system. The solid line in Figure 3 is a calculated scattering curve, assuming a Gaussian distribution of the tube radii, with a mean value of $\langle R \rangle = 26$ nm and a relative standard deviation of 8%. The obtained value of the radius is in excellent agreement with the cryo-TEM results. In the calculated curve, the resolution of the instrument has not been taken into account, and the 8% standard deviation is therefore expected to be an overestimate. The wall thickness is too thin to be obtained from the present SAXS data set. A finite thickness will result in a steeper q dependence at high q. In this case, essentially an overall q^{-2} decay within the whole q range is observed, from which it can be concluded that the wall thickness is smaller than ca. 1 nm.

In Figure 4, some scattering curves obtained at different concentrations are presented on the same graph. As can be seen, the scattering curves are very similar, demonstrating that the cylinder radius does not vary with the concentration in this concentration regime. The $\phi = 0.15$ sample scatters slightly differently at higher q. Here, the nanotube concentration is low, and we also see the scattering from the peptide monomers.

Because of the large radius−wall-thickness ratio, the packing density of the nanotubes increases rapidly with the effective peptide concentration. With a wall thickness of δ, the nanotube volume fraction is given by

$$\phi_{\text{tube}} = \frac{R}{2\delta}\phi_{\text{eff}} \tag{3}$$

where ϕ_{eff} is the effective peptide volume fraction (i.e., the volume fraction of peptides assembled in the tubes). This effective volume fraction is given by $\phi_{\text{eff}} = \phi - \phi_{\text{mon}}$, where ϕ is the total peptide volume fraction and ϕ_{mon} is the monomer volume fraction, which to a first approximation is

expected to be constant and equal to a critical aggregation concentration, ϕ_{cac}. This concentration appears to be very close to the volume fraction at the phase boundary (i.e., $\phi_{mon} \approx \phi_{cac} \approx 0.12$). Although an accurate value for the wall thickness has not yet been determined, the factor $R/2\delta$ is estimated to be larger than 10. The crowding observed in the cryo-TEM images (Figure 2) is significant, even though the effective peptide concentration is only a few percent. This also means that a close packing of the tubes is rapidly approached. The 2D hexagonal close packing is 81 vol %, and this value of ϕ_{eff} is expected to be reached when $\phi \approx 0.2$. Therefore, for higher peptide concentrations structural rearrangements are expected. This could be a deformation of the tube cross section into hexagons or the formation of multilayered tubes. The formation of multilayered tubes in this concentration regime is quite unlikely because the wall thickness is very small. Tube rigidity is an important parameter in this context. We have here assumed that the first liquid-crystalline phase formed is nematic. As the concentration is further increased, we also expect translational order and a transition to a hexagonal phase. This transition has recently been observed for a PEG peptide by Hamley et al.[17]

The self-assembly presented here is not gradual with dimers, trimers, and so forth. Instead, peptides self-assemble directly into very large structures when crossing a particular concentration, which is identified as the critical aggregation concentration, ϕ_{cac}. This implies that the self-assembly process is very cooperative. The observation is that the anisotropic phase is formed essentially as soon as nanotubes are formed. Hence, ϕ_{cac} is very close to the phase boundary of the liquid phase. The nanotubes are also very long and have a large aspect ratio, l/d, where l is the length and $d = 2R$ is the diameter. The tubes seen in Figure 2 are several micrometers long, which results in the aspect ratio l/d being approximately 50. Because of the large aspect ratio, there are strong excluded volume interactions, and the tubes are expected to form a nematic phase at low values of ϕ_{tube}. In Onsager's theory of the liquid-nematic transition of hard rods, phase boundaries occur at $\phi_L l/d = 3.34$ and $\phi_N l/d = 4.49$, where the concentration range $\phi_L \leq \phi_{tube} \leq \phi_N$ is the two-phase region between the liquid (L) and the nematic (N) phase, respectively. With $l/d \approx 50$, Onsager's theory[18] predicts a liquid-nematic transition at $\phi_{tube} \approx 0.07$. In this case, the tubes are also charged, which for the purely repulsive interaction means that the transition occurs at an even lower concentration.[19] As mentioned above, ϕ_{tube} grows very rapidly with increasing peptide concentration ϕ above ϕ_{cac}, with $\phi_{tube} = (R/2\delta)(\phi - \phi_{cac})$. With $R/2\delta \approx 10$, the transition is expected to occur at a peptide concentration of $\phi \approx \phi_{cac} + 0.007$ or even closer to ϕ_{cac} because of the electrostatic interactions. Work is in progress to identify a possible phase coexistence of disordered nanotubes and an ordered, nematic nanotube phase.

The present self-assembly is driven by hydrogen bonding. The self-assembly behavior here is different than for the N-terminus end-capped version of the same peptide that has been studied previously by Zhang et al.[20] With the end cap, A_6K becomes more amphiphilic, and Zhang et al. have reported on surfactant-like self-assembly behavior for that peptide where the driving force would be hydrophobic interactions.

In summary, we have investigated nanotube formation in a very simple peptide−water system. The nanotube self-assembly is characterized by a critical association and the formation of an ordered, presumably nematic, phase. This simple system lends itself to systematic investigations of peptide self-assembly, including the effects of peptide length by studying the homologous series A_nK. Such work is in progress.

Acknowledgment. We thank Gunnel Karlsson for her skillful assistance with the cryo-TEM experiments. This work was financially supported by the Swedish Research Council, including through the Linnaeus program Organizing Molecular Matter.

(17) Hamley, I. W.; Krysmann, M. J.; Castelletto, V.; Noirez, L. *Adv. Mater*. **2008**, *20*, 4394–4397.

(18) Onsager, L. *Ann. N.Y. Acad. Sci.* **1949**, *51*, 627.

(19) Stroobants, A.; Lekkerkerker, H. N. W.; Odijk, T. *Macromolecules* **1986**, *19*, 2232–2238.

(20) Vauthey, S.; Santoso, S.; Gong, H. Y.; Watson, N.; Zhang, S. G. *Proc. Natl. Acad. Sci. U.S.A.* **2002**, *99*, 5355–5360.